International Journal of Mechanical Sciences 000 (2018) 1–12

Contents lists available at ScienceDirect

International Journal of Mechanical Sciences

journal homepage: www.elsevier.com/locate/ijmecsci

Multibody simulation of railway vehicles with contact lookup tables

José L. Escalona [a,b], Javier F. Aceituno [c,*]

[a] Department of Engineering, Aarhus University, Denmark
[b] Mechanical and Manufacturing Engineering Department, University of Seville, Spain
[c] Mechanical and Mining Engineering Department, University of Jaén, Spain

ARTICLE INFO

Keywords:
Multibody railway dynamics
Contact lookup tables
Track irregularities
Symbolic computation
Efficient formulation

ABSTRACT

The use of contact lookup tables is widely used in multibody railway simulations to increase the computational efficiency. However, due to simplifying assumptions the use of contact lookup tables decreases the accuracy of the simulation results. This paper analyses the increase of computational efficiency and loss of accuracy for a particular multibody simulation. To this end the results based on contact lookup tables are compared with the results of the online solution of the wheel-rail contact constraints. The formulation used to compute the equations of motion of railway vehicles has the following features: (1) the equations of motion are obtained using a systematic procedure based on multibody dynamics, (2) generalized forces included in the equations of motion are obtained using symbolic computations when possible, (3) generalized coordinates are referred to a non-inertial track frame, (4) the equations of motion are obtained using a velocity transformation of the Newton–Euler equations of the vehicle bodies, which are assumed to be rigid and (5) wheel-rail tread contact and flange contact are treated with pre-calculated lookup tables which can take into account the track irregularities. The comparative study presented in this paper shows that this formulation can be used to simulate the dynamics of a railway vehicle in real-time.

1. Introduction

The interaction between railway vehicles and track has been of interest in many investigations through the literature generally by the use of multibody dynamics techniques [1]. It is a complex dynamical system in engineering because it can be defined by many bodies, include many degrees of freedom (DOFs) and involve a high degree of complexity. This is one of the reasons why dealing with efficient but accurate models that account for the dynamics of railroad vehicles is of great interest for the research community.

When modeling the dynamics of railroad vehicles, one has to consider the high computational cost that solving the non linearities of the multibody system entails. It is important to find an adequate formulation of the equations of motion and a proper integration method for its computer implementation [2]. In addition, special attention must be paid to the solution of the wheel-rail contact scenario since the analysis of the complex geometry of bodies in contact requires an important computational effort.

In multibody dynamics, the wheel-rail contact problem is one of the most fundamental issues for evaluating vehicle stability, ride comfort or curve negotiations [3]. It is assumed to occur at a single point where the normal and tangential contact forces are applied. In this context, two well-known and widely explained procedures can be used [4]; the Constraint Method, where the contact point is assumed to occur in a single point that occupies the same position in space for both bodies [5], and the Elastic Method, where the contact point in each body can occupy different position in space, allowing to occur indentation [6]. Both approaches are greatly time-consuming and as a consequence, many research publications focused on reliable efficient methods to evaluate the contact points locations can be found in the literature.

In general, the search of the contact points can be done in two ways: the online and the offline approach. In the online one, the location of the contact points is derived throughout the numeric simulation by solving the geometric equations that govern both the rigid or the elastic method. In [6], an optimized approach for searching all possible contact points in which each candidate point is grouped into a region of penetration called batch, is presented. In addition, Malvezzi et al. [7], presented two

Abbreviations: DOFs, Degrees of Freedom; GF, Global Frame; BF, Body Frame; TF, Track Frame; BTF, Body-Track Frame; WTF, Wheelset-Track Frame; WF, Wheelset Frame; WIF, Wheelset Intermediate Frame; DAE, Differential-algebraic equation; LU, Lookup tables; CC, Contact constraints.

* Corresponding author.
E-mail addresses: escalona@eng.au.dk (J.L. Escalona), jaceitun@ujaen.es (J.F. Aceituno).

https://doi.org/10.1016/j.ijmecsci.2018.01.020
Received 27 January 2017; Received in revised form 9 January 2018; Accepted 14 January 2018
Available online xxx
0020-7403/

semi-analytic procedures for the contact point detection between wheel and rail and based on the known analytic expressions of the surfaces in contact. One of these efficient semi-analytic methods is implemented in the work of Auciello et al. [8], where its computational efficiency is analyzed. Another interesting work related to the location of the wheel/rail contact points is presented by Sugiyama et al. [9], and it is based on the constraint formulation where tread, flange and back-of-flange contacts are allowed to be evaluated. Moreover, Recuero et al. [10], uses an accurate online elastic method that updates the geometry of the wheel-rail interface due to the rail flexibility.

With regard to the offline approach, which is used in this work, the concept of contact lookup table arises. A contact lookup table has solutions for specific wheelset positions relative to the track and can have their spatial derivatives and other geometric data associated with the contact points that are needed for the numerical simulations. Schupp et al. [11] proposed a quasi-elastic contact model that accounts qualitatively for the elastic deformation of the contact interface and approximates by two-dimensional splines the contact solution, whose coefficients are stored as a table in a pre-processing step. This method has been implemented in the commercial simulation package Simpack MBS [12]. Other works using the lookup table approach are those presented in [9,13,14]. In Meli et al. [13], the compass search together with the simplex numerical algorithm are used for the point detection, which is based on an analytical procedure that runs offline. Santamaría et al. [14] developed a procedure that accounts for the elastic contact in a lookup table approach. Here, four initial DOFs define the relative position of the wheelset with respect to the rail that are later reduced to three DOFs with the assumption that the contact point lies on radial sections at the wheel. Using an optimal number of discretized positions and the symmetric property of the problem, a reduced-size with 3-DOFs lookup table is obtained. Additionally, Sugiyama et al. [9] developed a hybrid procedure to account for the contact points both online and offline, in which a lookup table is used for evaluating the candidate points in the wheel tread while an iterative search is employed for predicting flange contact.

When evaluating the wheel-rail contact points, it is of major importance to include the effect of track irregularities, since its locations are highly influenced by these defects. However, the consideration of track irregularities when using contact lookup tables, as it is presented in further sections of this work, is a difficult task. Despite it allows a great reduction in the computational cost, it also augments the number of independent variables or entries to the table. Therefore, an efficient and simple solution to account for track irregularities when using contact lookup tables is proposed.

The goal of this paper is to develop a detailed, systematic, efficient and real-time capable procedure based on multibody dynamics to obtain the equations of motion of railway vehicles using pre-calculated contact lookup tables that account for track irregularities. To this end, this paper is described as follows: Section 2 summarizes the coordinates and reference frames used in the formulation of railway vehicles. Section 3 details the adopted notation and the kinematic description of vehicle bodies and moving frames employed. In addition, symbolic computations of the kinematic terms are derived when possible. Section 4 contains the Newton—Euler equations of motion for railroad vehicles while Section 5 presents a method to use relative coordinates associated with the kinematic joints to model the relative motion between group of bodies avoiding the use of constraints. This method is applied to a wheelset—two axleboxes group of bodies and to a carbody—two bogie frame. In Section 6, the innovative contact lookup table based on the constraint approach that accounts for track irregularities is presented. Finally, Section 7 provides the numerical solution when the proposed formulation is applied to a railway vehicle. A comparison of the efficient computational cost when using contact lookup tables is also developed and analyzed with respect to its loss in accuracy when the online constraint approach is used.

2. Coordinates and frames in multibody railway dynamics

In multibody dynamics the coordinates that are used to describe the motion of the bodies are used to obtain the position and orientation of the *body frame* (BF) with respect to an inertial and *global frame* (GF). Two families of coordinates can be used: reference coordinates, that include a fixed set of position and orientation coordinates for each of the bodies with respect to the inertial frame, and relative or joint coordinates that describe the position and orientation of the bodies with respect to other moving bodies. Pros and cons of both approaches are well known.

If the multibody system is a ground vehicle that follows a guideway (road for cars or track for trains [15]) an intermediate frame that is neither inertial nor body fixed can be defined for a convenient description of the motion of the bodies. This frame advances along the guideway with approximately the same forward velocity as the vehicle. In this paper that is devoted to railway dynamics this frame is called *track frame* (TF). The use of the TF does not exclude the definition of the GF that is always needed when using Newton laws. The position and orientation of the TF with respect to the inertial frame is a function of the guideway geometry and is usually obtained as a function of an arc-length coordinate. In a track frame formulation body coordinates describe the position and orientation of the BF with respect to the TF. These coordinates are called here *track coordinates*. The main advantages of the use of track coordinates are:

1. When using the TF the magnitude of the coordinates of the bodies remains bounded while they may grow with no limit when this frame is not used. The accuracy in the description of the relative motion decreases as the absolute value of the coordinates increases.
2. Steady motion of the vehicle like steady curving can be described with a set of constant coordinates when using the track coordinates [16].
3. As a consequence of the previous point, stability analysis of steady motions can be analyzed by simple linearization and eigenvalue analysis when using the TF. When using the inertial frame similar analysis require the more expensive simulation-based “brute force” approach or the more difficult stability of limit cycles [16].
4. Constrained motion of the vehicle bodies with respect to the guideway, like the forward velocity constraint, is easily imposed [3] using track coordinates.

On the other hand, the use of track coordinates shows the following drawbacks:

1. The kinematic description of the bodies is much more complicated because it involves the guideway geometry. The calculation of velocities and acceleration of the bodies require the calculation of partial derivatives of the guideway geometry with respect to the TF arc-length coordinate. These expressions enter in the vehicle equations of motion becoming computationally more expensive.
2. General purpose multibody codes that include special modules for the analysis of ground vehicles require different functions for the evaluation of common generalized forces like, for instance, these due to spring-dashpot elements (suspensions) when track coordinates are used.

The reference coordinates of an arbitrary body i with respect to the GF used in general-purpose multibody dynamics are:

$$\mathbf{q}^i = [\mathbf{R}^{iT} \quad \boldsymbol{\theta}^{iT}]^T \tag{1}$$

where $\mathbf{R}^i$ is the position vector and $\boldsymbol{\theta}^i$ is a set of orientation coordinates of the BF. When the TF is used the motion of each vehicle body is accompanied by a TF along the track. We call this frame here the body-track frame (BTF), see Fig. 1. The track coordinates of the vehicle bodies are usually defined as:

$$\mathbf{q}^i = [s^i \quad r_y^{t,i} \quad r_z^{t,i} \quad \boldsymbol{\theta}^{t,iT}]^T \tag{2}$$

where s^i is the arc-length coordinate of body i along the track, $r_y^{t,i}$ and $r_z^{t,i}$ are the body frame position components with respect to the BTF

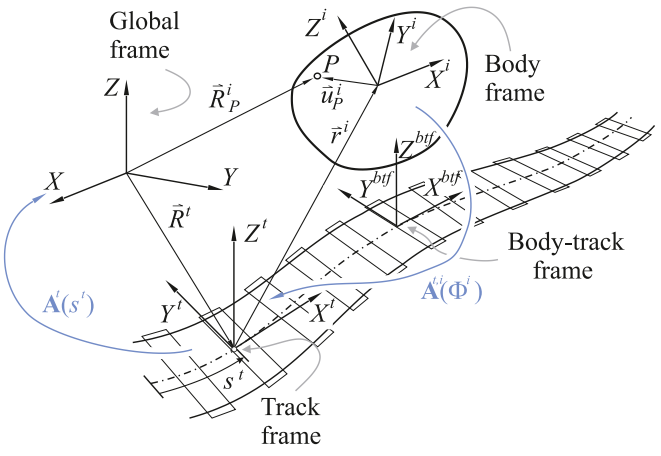

Fig. 1. Frames and coordinates for the kinematic description of vehicle bodies: global frame, track frame, body-track frame and body frame.

($r_x^{t,i}$ is assumed to be zero) and $\boldsymbol{\theta}^{t,i}$ is a set of orientation coordinates of the BF with respect to the BTF.

In the formulation described in this work a single TF for the whole vehicle is proposed. BTF's are needed too. However, the set of coordinates used for the kinematic description of the vehicle bodies do not refer to the BTF as in Eq. (2) as shown in next section. This fact alleviates the drawbacks of the use of the track coordinates described previously.

In this work the different bodies used to model railway vehicles are divided into two groups: wheelsets (superscript "*w*" is used for them) and non-wheelset bodies (superscript "*nw*" is used for them). The obvious difference is that wheelset bodies undergo large pitch rotation while non-wheelset bodies do not. For wheelset kinematics it is convenient to define a *wheelset intermediate frame* (WIF) that accompanies the motion of the wheelset with the exception of large pitch rotation. The precise definition of this frame is given in next section.

3. Kinematics

This section explains in detail kinematic description used in the multibody Track Frame Formulation used in this work for the modeling and simulation of the dynamics of railway vehicles.

3.1. Vectors and frames

In this work the following symbols are used to express position vectors in different frames:

1. $\vec{R}$ is a position vector whose origin is attached to the GF.
2. $\vec{r}$ is a position vector whose origin is attached to the TF.
3. $\vec{u}$ is a position vector whose origin is attached to the BF.
4. $\vec{b}$ is a position vector whose origin is attached to the BTF.

On the other hand, the following symbols are used to express the vector components given in the different frames:

1. Bold symbols without superscript, like $\mathbf{v}$, mean the 3×1 column matrix that contains the components of vector $\vec{v}$ in the GF.
2. Bold symbols with 'bar' superscript, like $\bar{\mathbf{v}}$, mean the 3×1 column matrix that contains the components of vector $\vec{v}$ in the TF.
3. Bold symbols with 'hat' superscript, like $\hat{\mathbf{v}}$, mean the 3×1 column matrix that contains the components of vector $\vec{v}$ in the BF (being the WF for wheelset bodies).
4. Bold symbols with 'arc' superscript, like $\overset{\frown}{\mathbf{v}}$, mean the 3×1 column matrix that contains the components of vector $\vec{v}$ in the BTF (WTF in case of a wheelset).
5. Bold symbols with 'inverted arc' superscript, like $\overset{\smile}{\mathbf{v}}$, mean the 3×1 column matrix that contains the components of vector $\vec{v}$ in the WIF.

3.2. Kinematics of the TF

The TF $[O^t\ (X^t\ Y^t\ Z^t)]$ is assumed to follow the track center line keeping axis X^t tangent to the track centerline. Axis Y^t connects the two rails centerlines. The arc length along the track centerline traveled by the TF is denoted as s^t. The coordinates that describe the position of the origin and orientation of the TF with respect to the GF are:

$$\mathbf{q}^t = \begin{bmatrix} x^t & y^t & z^t & \varphi^t & \theta^t & \psi^t \end{bmatrix}^T \tag{3}$$

where $\mathbf{R}^t = [x^t\quad y^t\quad z^t]^T$ is the position vector of the origin of the TF O^t with respect to the GF and $\boldsymbol{\Phi}^t = [\varphi^t\quad \theta^t\quad \psi^t]^T$ is a set of three Euler angles that describe the orientation of the TF with respect to the GF. The coordinates of the TF are known functions of the track centerline geometry, this is, $\mathbf{q}^t = \mathbf{q}^t(s^t)$. Therefore, the set of coordinates shown in Eq. (3) cannot be considered as part of the system coordinates. The arc-length coordinate s^t is in fact the only coordinate that shows the gross forward motion of the vehicle along the track. This coordinate is usually kinematically constrained in many railway applications with the so-called *forward velocity constraint* that established the forward motion of the vehicle.

3.3. Kinematics of a vehicle body

The position and orientation of the BF $[O^i\ (X^i\ Y^i\ Z^i)]$ of a body i of the vehicle with respect to the TF is defined with the coordinates:

$$\mathbf{q}^i = \begin{bmatrix} x^i & y^i & z^i & \varphi^i & \theta^i & \psi^i \end{bmatrix}^T \tag{4}$$

where $\bar{\mathbf{r}}^i = [x^i\quad y^i\quad z^i]^T$ is the position vector of the origin of the BF O^i with respect to the TF and $\boldsymbol{\Phi}^i = [\varphi^i\quad \theta^i\quad \psi^i]^T$ is a set of three Euler angles that describe the orientation of the BF with respect to the TF. Note that the superscript "*t,i*" used in Eq. (2) that stands for "position or orientation of BF i with respect to the TF t" has been substituted by simply '*i*' for the sake of simplicity of the notation. On the other hand, the set of coordinates included in Eq. (2) combines an absolute and relative coordinates while the set of coordinates in Eq. (4) includes only relative coordinates.

The position vector $\mathbf{R}^i_P$ of an arbitrary point P of body i with respect to the GF is given by:

$$\begin{aligned} \mathbf{R}^i_P &= \mathbf{R}^t + \mathbf{A}^t\bar{\mathbf{r}}^i_P \\ \bar{\mathbf{r}}^i_P &= \bar{\mathbf{r}}^i + \mathbf{A}^{t,i}\hat{\mathbf{u}}^i_P \end{aligned} \tag{5}$$

where $\bar{\mathbf{r}}^i_P$ is the position vector of P with respect to the TF and $\hat{\mathbf{u}}^i_P$ is the position vector of point P with respect to the BF (see Fig. 1).

3.4. Wheelset kinematics

Three different frames are used for the wheelset kinematic description (see Fig. 2) namely:

1. Wheelset body frame (WF) $[O^w\ (X^w\ Y^w\ Z^w)]$ whose orientation with respect to the TF is given by the Euler angles $\boldsymbol{\Phi}^w = [\varphi^w\quad \theta^w\quad \psi^w]^T$. WF is the name given to the BF when the body is a wheelset.
2. Wheelset intermediate frame (WIF) $[O^{wif}\ (X^{wif}\ Y^{wif}\ Z^{wif})]$ whose orientation with respect to the TF is given by the Euler angles $\boldsymbol{\Phi}^{wif} = [\varphi^w\quad 0\quad \psi^w]^T$. This is, the WF is the result of rotating the WIF the pitch angle θ^w about the common Y^w axis.
3. Wheelset-track frame (WTF) $[O^{wft}\ (X^{wft}\ Y^{wft}\ Z^{wtf})]$ that accompanies the wheelset along the track centerline. WTF is the name given to the BTF when the body is a wheelset.

The definition of the WTF is convenient to define the motion of the wheelset with respect to the track and also for the numerical treatment of the wheel-rail contact with lookup tables. In what follows the calculation of the position and orientation of the WTF with respect to the TF once the values of the coordinates $\mathbf{q}^w$ and $\mathbf{q}^t$ are known is presented.

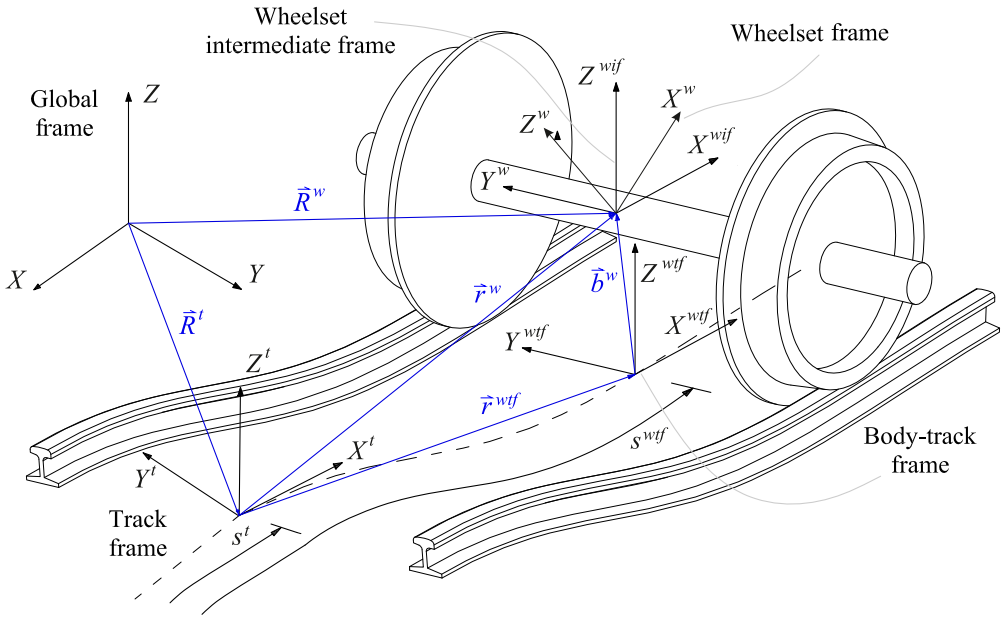

Fig. 2. Additional frames for the kinematic description of a wheelset body: wheelset-body frame, wheelset-intermediate frame and wheelset-track frame.

These calculations are just the same for any other BTF (for non-wheelset bodies.)

In order to find the position and orientation of the WTF an arc-length parameter s^{wtf} has to be associated at any time with each wheelset. This parameter is the arc length along the track centerline of the WTF. Given the coordinates of the WF $\mathbf{q}^w$ and the TF $\mathbf{q}^t$, the calculation of s^{wft} requires the solution of the following non-linear algebraic equation:

$$\mathbf{i}^{tcl}\left(s^{wtf}\right)^T\left(\mathbf{R}^w - \mathbf{R}^{tcl}\left(s^{wtf}\right)\right) = 0 \tag{6}$$

where $\mathbf{R}^{tcl}(s)$ and $\mathbf{i}^{tcl}(s)$ are the functions that provide the position and tangent vector of a point in the track centerline ($tcl = track\ centerline$) given the arc length s. Eq. (6) states that the position vector $\mathbf{r}^{wif}$ ($= \mathbf{R}^w - \mathbf{R}^{tcl}$) of the WIF with respect to the WTF is perpendicular to the tangent to the track at the body location. In other words, it states that the position vector has zero X coordinate in the WTF.

In a tangent track the body arc-length parameter s^{wtf} coincides with ($s^t + x^w$). In this case it is not required to solve Eq. (6) to find the value of s^{wtf}. For a circular track one can find an analytical expression that provides the value of s^{wtf} without solving Eq. (6). In other situations, for example when the TF is in a tangent rail whereas the wheelset is at a transition or curved rail, Eq. (6) should be solved to find the value of s^{wtf}. Alternatively, ($s^{wtf} - s^t$) can be considered as constant throughout the simulation thus avoiding the solution of Eq. (6) each time step. This alternative neglects the influence of the vehicle longitudinal dynamics in the position of WTF with respect to the TF.

Once the wheelset arc-length parameter s^{wtf} has been calculated, the position of the origin $\bar{\mathbf{r}}^{wtf}$ and the transformation matrix $\mathbf{A}^{t,wtf}$ from the WTF to the TF can be calculated using the rail preprocessor.

In addition to the wheelset generalized coordinates $\mathbf{q}^w$ that include the position and orientation of the wheelset with respect to the TF as shown in Eq. (4), the set of coordinates $\mathbf{q}^{wif}$ that describe the position and orientation of the WIF with respect to the WTF need to be calculated during the dynamic simulation. This set of coordinates can be calculated as a function of $\mathbf{q}^w$ once the position of WTF is obtained. Coordinates of $\mathbf{q}^{wif}$ are 5 instead of 6, as follows:

$$\mathbf{q}^{wif} = [y^{wif} \quad z^{wif} \quad \varphi^{wif} \quad \theta^{wif} \quad \psi^{wif}]^T \tag{7}$$

The position and orientation of the WIF with respect to the WTF is a function of this set of coordinates, as follows:

$$\widehat{\mathbf{b}}^w = \begin{bmatrix} 0 \\ y^{wif} \\ z^{wif} \end{bmatrix}, \quad \mathbf{A}^{wtf,wif} = \begin{bmatrix} 1 & -\psi^{wif} & \theta^{wif} \\ \psi^{wif} & 1 & -\varphi^{wif} \\ -\theta^{wif} & \varphi^{wif} & 1 \end{bmatrix} \tag{8}$$

where small-angles assumption is used. In order to calculate $\mathbf{q}^{wif}$ from $\mathbf{q}^w$, $\mathbf{q}^t(s^t)$ and $\mathbf{q}^{wtf}(s^{wtf})$ the following simple relative kinematics equations are inverted:

$$\left.\begin{aligned} \bar{\mathbf{r}}^w &= \bar{\mathbf{r}}^{wtf} + \mathbf{A}^{t,wtf}\,\widehat{\mathbf{b}}^w \\ \mathbf{A}^{t,wif} &= \mathbf{A}^{t,wtf}\mathbf{A}^{wtf,wif} \end{aligned}\right\} \Rightarrow \left\{\begin{aligned} \widehat{\mathbf{b}}^{\mathbf{w}} &= \mathbf{A}^{t,wtf^T}\left(\bar{\mathbf{r}}^w - \bar{\mathbf{r}}^{wtf}\right) \\ \mathbf{A}^{wtf,wif} &= \mathbf{A}^{t,wtf^T}\mathbf{A}^{t,wif} \end{aligned}\right. \tag{9}$$

Using the expressions on the right hand side one can easily extract the coordinates $\mathbf{q}^{wif}$. The convenience of the reasonable small-angles assumptions of the WIF with respect to the WTF is clear in order to get the angles from $\mathbf{A}^{wtf,wif}$ avoiding complex trigonometric expressions. This assumption is very useful for imposing contact constraints with lookup tables as explained in Section 6.

3.5. Symbolic calculation of velocities and accelerations

Once the position of an arbitrary point of a vehicle body is defined by Eq. (5) and the rotation matrix of the vehicle body BF is obtained from $\mathbf{\Phi}^i$, the calculation of the velocity and acceleration of an arbitrary point and the calculation of the angular velocity and angular acceleration of the body are obtained using symbolic computation. To this end, the following kinematic relations are used:

$$\dot{\mathbf{R}}^i_P = \frac{\partial \mathbf{R}^i_P}{\partial \mathbf{q}^t}\dot{\mathbf{q}}^t + \frac{\partial \mathbf{R}^i_P}{\partial \mathbf{q}^i}\dot{\mathbf{q}}^i = \mathbf{H}^{t/i}_P\dot{\mathbf{q}}^t + \mathbf{H}^i_P\dot{\mathbf{q}}^i \tag{10}$$

where

$$\mathbf{H}^{t/i}_P = \frac{\partial \mathbf{R}^i_P}{\partial \mathbf{q}^t}, \quad \mathbf{H}^i_P = \frac{\partial \mathbf{R}^i_P}{\partial \mathbf{q}^i} \tag{11}$$

are the 3×6 Jacobian matrices that can be evaluated symbolically from Eq. (5). Both matrices are functions of $\mathbf{q}^t$ and $\mathbf{q}^i$. The acceleration of point P is obtained as:

$$\ddot{\mathbf{R}}^i_P = \mathbf{H}^{t/i}_P\ddot{\mathbf{q}}^t + \mathbf{H}^i_P\ddot{\mathbf{q}}^i + \mathbf{h}^{t/i}_P\dot{\mathbf{q}}^t + \mathbf{h}^i_P\dot{\mathbf{q}}^i \tag{12}$$

where the following Jacobian matrices are used:

$$\mathbf{h}^{t/i}_P = \frac{\partial \dot{\mathbf{R}}^i_P}{\partial \mathbf{q}^t}, \quad \mathbf{h}^i_P = \frac{\partial \dot{\mathbf{R}}^i_P}{\partial \mathbf{q}^i} \tag{13}$$

As it will be shown in later sections, during the calculation of the vehicle equations of motion, the inertia forces of the vehicle bodies are projected in the TF. To this end, the expression of the absolute acceleration of the center of gravity G of body i projected to the TF is needed. This expression takes the form:

$$\ddot{\bar{\mathbf{R}}}_G^i = \mathbf{A}^{tT}\ddot{\mathbf{R}}_G^i = \bar{\mathbf{H}}_G^{t/i}\ddot{\mathbf{q}}^t + \bar{\mathbf{H}}_G^i\ddot{\mathbf{q}}^i + \bar{\mathbf{h}}_G^{t/i}\dot{\mathbf{q}}^t + \bar{\mathbf{h}}_G^i\dot{\mathbf{q}}^i \tag{14}$$

where

$$\bar{\mathbf{H}}_G^{t/i} = \mathbf{A}^{tT}\mathbf{H}_G^{t/i},\ \bar{\mathbf{H}}_G^i = \mathbf{A}^{tT}\mathbf{H}_G^i,\ \bar{\mathbf{h}}_G^{t/i} = \mathbf{A}^{tT}\mathbf{h}_G^{t/i},\ \bar{\mathbf{h}}_G^i = \mathbf{A}^{tT}\mathbf{h}_G^i \tag{15}$$

As it will be shown in later sections, for the calculation of the vehicle equations of motion, the moment of the inertia forces of the non-wheelset vehicle bodies are projected to the BF. To this end, the expression of the absolute angular acceleration of the non-wheelset body i projected to the BF is needed. Therefore, the symbolic calculation of the angular velocities and accelerations of vehicle bodies projected to the BF is explained next. The absolute angular velocity of a vehicle body is calculated as the sum of the BF angular velocity with respect to the TF plus the angular velocity of the TF with respect to the GF, as follows:

$$\hat{\boldsymbol{\omega}}^i = \mathbf{A}^{tT}\boldsymbol{\omega}^t + \hat{\boldsymbol{\omega}}^{t,i} \tag{16}$$

where $\mathbf{A}^i = \mathbf{A}^t\mathbf{A}^{t,i}$. The angular velocity vectors are obtained from the following well-known formulas:

$$\begin{aligned}\boldsymbol{\omega}^t &= \text{axial}\left(\dot{\mathbf{A}}^t\mathbf{A}^{tT}\right)\\ \hat{\boldsymbol{\omega}}^{t,i} &= \text{axial}\left(\mathbf{A}^{t,iT}\dot{\mathbf{A}}^{t,i}\right)\end{aligned} \tag{17}$$

The angular acceleration takes the form:

$$\hat{\boldsymbol{\alpha}}^i = \dot{\hat{\boldsymbol{\omega}}}^i = \hat{\mathbf{G}}^{t/i}\ddot{\mathbf{q}}^t + \hat{\mathbf{G}}^i\ddot{\mathbf{q}}^i + \hat{\mathbf{g}}^{t/i}\dot{\mathbf{q}}^t + \hat{\mathbf{g}}^i\dot{\mathbf{q}}^i \tag{18}$$

where the following Jacobian matrices are used:

$$\hat{\mathbf{G}}^{t/i} = \frac{\partial\hat{\boldsymbol{\omega}}^i}{\partial\dot{\mathbf{q}}^t},\ \hat{\mathbf{G}}^i = \frac{\partial\hat{\boldsymbol{\omega}}^i}{\partial\dot{\mathbf{q}}^i},\ \hat{\mathbf{g}}^{t/i} = \frac{\partial\hat{\boldsymbol{\omega}}^i}{\partial\mathbf{q}^t},\ \hat{\mathbf{g}}^i = \frac{\partial\hat{\boldsymbol{\omega}}^i}{\partial\mathbf{q}^i} \tag{19}$$

However, for the vehicle wheelsets Euler equations are projected to the WIF. This is convenient because the contact forces do not rotate in this frame as they do in the WF. The angular velocity of the wheelset projected to the WIF takes the form:

$$\breve{\boldsymbol{\omega}}^w = \mathbf{A}^{wifT}\boldsymbol{\omega}^t + \breve{\boldsymbol{\omega}}^{t,w} \tag{20}$$

where matrix $\mathbf{A}^{wif} = \mathbf{A}^t\mathbf{A}^{t,wif}$ is the rotation matrix from the WIF to the GF. The angular acceleration of the wheelset projected to the WIF yields:

$$\breve{\boldsymbol{\alpha}}^w = \dot{\breve{\boldsymbol{\omega}}}^w = \breve{\mathbf{G}}^{t/w}\ddot{\mathbf{q}}^t + \breve{\mathbf{G}}^w\ddot{\mathbf{q}}^i + \breve{\mathbf{g}}^{t/w}\dot{\mathbf{q}}^t + \breve{\mathbf{g}}^w\dot{\mathbf{q}}^w \tag{21}$$

where the following Jacobian matrices are used:

$$\breve{\mathbf{G}}^{t/w} = \frac{\partial\breve{\boldsymbol{\omega}}^w}{\partial\dot{\mathbf{q}}^t},\ \breve{\mathbf{G}}^w = \frac{\partial\breve{\boldsymbol{\omega}}^w}{\partial\dot{\mathbf{q}}^w},\ \breve{\mathbf{g}}^{t/w} = \frac{\partial\breve{\boldsymbol{\omega}}^w}{\partial\mathbf{q}^t},\ \breve{\mathbf{g}}^w = \frac{\partial\breve{\boldsymbol{\omega}}^w}{\partial\mathbf{q}^w} \tag{22}$$

4. Dynamics

4.1. Newton–Euler equations for vehicle bodies

The equations of motion of the railroad vehicles obtained in this work are based on the Newton–Euler equations of the rigid bodies that comprise the vehicle. Newton equations are projected to the TF, as follows:

$$m^i\ddot{\bar{\mathbf{R}}}_G^i = \bar{\mathbf{F}}^i \tag{23}$$

where $\ddot{\bar{\mathbf{R}}}_G^i$ is the acceleration of the center of gravity of body i as given in Eq. (14) and $\bar{\mathbf{F}}^i$ is the sum of all forces applied to the body projected to the TF. This force vector includes applied forces (gravity force, suspension forces, aerodynamic forces and contact forces) and reaction forces associated with constraints due to kinematic joints or other assumed rheonomic constraints. For non-wheelset bodies Euler equations are projected to the BF, as follows:

$$\hat{\mathbf{I}}^{nw}\hat{\boldsymbol{\alpha}}^{nw} = \hat{\mathbf{T}}^{nw} - \hat{\boldsymbol{\omega}}^{nw}\times\left(\mathbf{I}^{nw}\hat{\boldsymbol{\omega}}^{nw}\right) \tag{24}$$

where $\hat{\boldsymbol{\omega}}^{nw}$ and $\hat{\boldsymbol{\alpha}}^{nw}$ are the angular velocity and angular acceleration vector as given by Eqs. (16) and (18), respectively, $\hat{\mathbf{I}}^{nw}$ is the inertia tensor of the non-wheelset body in the BF and $\hat{\mathbf{T}}^{nw}$ is the vector sum of moments applied with respect to the center of gravity projected to the BF. In the case of the wheelsets, Euler equations are projected to the WIF, as follows:

$$\breve{\mathbf{I}}^w\breve{\boldsymbol{\alpha}}^w = \breve{\mathbf{T}}^w - \breve{\boldsymbol{\omega}}^w\times\left(\mathbf{I}^w\breve{\boldsymbol{\omega}}^w\right) \tag{25}$$

where $\breve{\boldsymbol{\omega}}^w$ and $\breve{\boldsymbol{\alpha}}^w$ are the angular velocity and angular acceleration vector as given by Eqs. (20) and (21), respectively, $\breve{\mathbf{I}}^w$ is the inertia tensor of the wheelset body in the WIF and $\breve{\mathbf{T}}^w$ is the vector sum of moments applied with respect to the center of gravity projected to the WIF. Because the wheelset is a solid of revolution with two planes of symmetry such that $I_x = I_z$, the inertia tensor in the WIF coincides with the inertia tensor in the WF, being both constant tensors.

The Newton–Euler equations for the non-wheelset vehicle bodies yield:

$$\begin{bmatrix} m^i\mathbf{1} & \mathbf{0}\\ \mathbf{0} & \hat{\mathbf{I}}^{ni}\end{bmatrix}\begin{bmatrix}\ddot{\bar{\mathbf{R}}}_G^i\\ \hat{\boldsymbol{\alpha}}^i\end{bmatrix} = \begin{bmatrix}\bar{\mathbf{F}}^i\\ \hat{\mathbf{T}}^i\end{bmatrix} + \begin{bmatrix}\mathbf{0}\\ -\hat{\boldsymbol{\omega}}^i\times\left(\hat{\mathbf{I}}^i\hat{\boldsymbol{\omega}}^i\right)\end{bmatrix} \Rightarrow \mathbf{M}_{NE}^i\mathbf{a}^i = \mathbf{Q}_{NE}^i + \mathbf{Q}_{v\,NE}^i \tag{26}$$

where $\mathbf{M}_{NE}^i$ is the Newton–Euler mass matrix, $\mathbf{a}^i$ is the vector that contains the translational and angular acceleration of the body (which does not coincide with the second derivative of the body coordinates), $\mathbf{Q}_{NE}^i$ is the vector of Newton–Euler generalized forces and $\mathbf{Q}_{v\,NE}^i$ is the Newton–Euler quadratic-velocity generalized inertia forces. This equation is also valid for the wheelsets if Euler Eq. (25) is used instead of Eq. (24). Combining Eq. (14) and Eq. (18), the vector of accelerations is given by:

$$\begin{aligned}\mathbf{a}^i &= \begin{bmatrix}\ddot{\bar{\mathbf{R}}}_G^i\\ \hat{\boldsymbol{\alpha}}^i\end{bmatrix} = \begin{bmatrix}\bar{\mathbf{H}}_G^{t/i}\\ \hat{\mathbf{G}}^{t/i}\end{bmatrix}\ddot{\mathbf{q}}^t + \begin{bmatrix}\bar{\mathbf{H}}_G^i\\ \hat{\mathbf{G}}^i\end{bmatrix}\ddot{\mathbf{q}}^i + \begin{bmatrix}\bar{\mathbf{h}}_G^{t/i}\\ \hat{\mathbf{g}}^{t/i}\end{bmatrix}\dot{\mathbf{q}}^t + \begin{bmatrix}\bar{\mathbf{h}}_G^i\\ \hat{\mathbf{g}}^i\end{bmatrix}\dot{\mathbf{q}}^i\\ &= \mathbf{L}^{t/i}\ddot{\mathbf{q}}^t + \mathbf{L}^i\ddot{\mathbf{q}}^i + \mathbf{l}^{t/i}\dot{\mathbf{q}}^t + \mathbf{l}^i\dot{\mathbf{q}}^i\end{aligned} \tag{27}$$

where the 6×6 Jacobian matrices $\mathbf{L}^{t/i}$, $\mathbf{L}^i$, $\mathbf{l}^{t/i}$ and $\mathbf{l}^i$ assemble the 3×6 Jacobian matrices previously defined that are computed symbolically. Introducing Eq. (27) in Eq. (26) and rearranging yields:

$$\mathbf{M}_{NE}^i\mathbf{L}^i\ddot{\mathbf{q}}^i = \mathbf{Q}_{NE}^i + \mathbf{Q}_{v\,NE}^i - \mathbf{M}_{NE}^i\left(\mathbf{L}^{t/i}\ddot{\mathbf{q}}^t + \mathbf{l}^{t/i}\dot{\mathbf{q}}^t + \mathbf{l}^i\dot{\mathbf{q}}^i\right) \tag{28}$$

Premultiplying this equation by $\mathbf{L}^{iT}$ and rearranging yields:

$$\mathbf{M}^i\ddot{\mathbf{q}}^i = \mathbf{Q}^i + \mathbf{Q}_v^i + \mathbf{Q}_{TFin}^i \tag{29}$$

where the mass matrix and force vectors are defined as follows:

$$\begin{aligned}&\mathbf{M}^i = \mathbf{L}^{iT}\mathbf{M}_{NE}^i\mathbf{L}^i,\ \mathbf{Q}^i = \mathbf{L}^{iT}\mathbf{Q}_{NE}^i,\\ &\mathbf{Q}_v^i = \mathbf{L}^{iT}\left(\mathbf{Q}_{vNE}^i - \mathbf{M}_{NE}^i\mathbf{l}^i\dot{\mathbf{q}}^i\right),\ \mathbf{Q}_{TFin}^i = -\mathbf{L}^{iT}\mathbf{M}_{NE}^i(\mathbf{L}^{t/i}\ddot{\mathbf{q}}^t + \mathbf{l}^{t/i}\dot{\mathbf{q}}^t)\end{aligned} \tag{30}$$

In this equation matrix $\mathbf{M}^i$ is the mass matrix, $\mathbf{Q}^i$ is the vector of generalized forces, $\mathbf{Q}_v^i$ is the vector of quadratic velocity inertia forces due to the BF to TF relative motion and $\mathbf{Q}_{TFin}^i$ is the vector of inertia forces due to the TF motion.

4.2. Equations of motion of railway vehicles

For a general railroad vehicle, the relative motion of some vehicle bodies can be constrained due to kinematic joints such as revolute, spherical, prismatic or cylindrical joints [17]. However, some simplified vehicle models assume that the relative motion of all vehicle bodies is unconstrained being their interaction due to spring-dashpot suspension elements [3]. For these *unconstrained vehicles* the equations of motion are

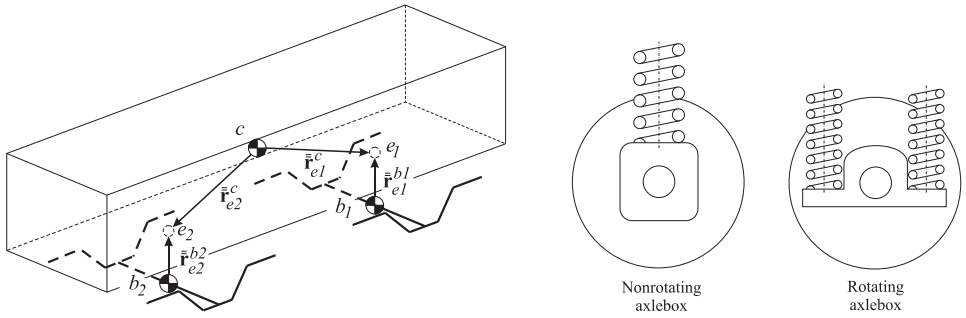

Fig. 3. Open-tree chains of bodies in railway vehicles. Left: carbody-bogie chain. Right: wheelset-axlebox chain.

simply obtained by assembling the equations of motion of the vehicle bodies as given at Eq. (29). The equations of motion of the unconstrained vehicle are given by:

$$\mathbf{M}\ddot{\mathbf{q}} = \mathbf{Q} + \mathbf{Q}_v + \mathbf{Q}_{TFin} + \mathbf{Q}_{susp} \tag{31}$$

where the mass matrix and force vectors are defined as follows:

$$\mathbf{M} = \begin{bmatrix} \mathbf{M}^2 & & & \\ & \mathbf{M}^3 & & \\ & & \ddots & \\ & & & \mathbf{M}^{nb} \end{bmatrix}, \quad \mathbf{Q} = \begin{bmatrix} \mathbf{Q}^2 \\ \mathbf{Q}^3 \\ \vdots \\ \mathbf{Q}^{nb} \end{bmatrix}, \quad \mathbf{Q}_v = \begin{bmatrix} \mathbf{Q}_v^2 \\ \mathbf{Q}_v^3 \\ \vdots \\ \mathbf{Q}_v^{nb} \end{bmatrix}, \quad \mathbf{Q}_{TFin} = \begin{bmatrix} \mathbf{Q}_{TFin}^2 \\ \mathbf{Q}_{TFin}^3 \\ \vdots \\ \mathbf{Q}_{TFin}^{nb} \end{bmatrix} \tag{32}$$

and $\mathbf{Q}_{susp}$ is the vector of generalized suspension forces. Vector of generalized forces $\mathbf{Q}$ that appear in Eq. (31) includes *applied forces* and *reaction forces*, $\mathbf{Q} = \mathbf{Q}_{app} + \mathbf{Q}_{reac}$. Applied forces are those that can be calculated as a function of the system generalized coordinates, generalized velocities and time. Reaction forces appear under the presence of kinematic constraints in the system coordinates. Eq. (31) cannot be solved directly because reaction forces are unknown. For their solution this set of equations has to be transformed to a system of *differential-algebraic equations* (DAE) first using the method of the Lagrange multipliers to account for the reaction forces.

In railway vehicles the kinematic constraints can be due to the presence of joints between different bodies that eliminates certain relative motions and also due to the wheel-rail contact. The treatment of these two types of constraints is different in the method proposed in this work. Next two sections explain it in detail.

5. Models for railway vehicles with joint constraints

As said in Section 4, the relative motion of some railroad vehicle bodies can be constrained due to the existence of different kinematic joints such as revolute, spherical, prismatic or cylindrical joints. The coordinates selection and kinematics proposed in Section 3 is not efficient in this case because of the appearance of non-linear constraints that can be avoided. The method proposed in this work uses relative coordinates associated with the kinematic joints to model the relative motion thus avoiding the use of constraints. For the sake of computational efficiency, the kinematics of groups of bodies that can be considered as open chain mechanism is modeled as a whole. In these kinematic chains one of the bodies is considered as the base body. The set of coordinates associated with the chain of bodies include the coordinates of the base body frame with respect to the TF and the relative coordinates of the rest of the bodies with respect to the base body. Two examples of common groups of bodies that appear in railroad vehicles are used as examples: the carbody connected by spherical joints to two bogie frames and the wheelset connected by revolute joints to two axleboxes.

The mechanical connection between the bogie frame and the carbody is sometimes modeled as a spherical or cylindrical joint, see Fig. 3 on the left. Assuming that the spherical joint models that connection (see Fig. 3 on the left, where e_1 and e_2 refer to the spherical joints), the group of bodies formed by the carbody c, that is used as base body, and the bogie frames b_1 and b_2 can be kinematically described using the following vector of coordinates:

$$\begin{aligned} \mathbf{q}^{CB} &= \begin{bmatrix} x^c & y^c & z^c & \varphi^c & \theta^c & \psi^c & \varphi^{e1} & \theta^{e1} & \psi^{e1} & \varphi^{e2} & \theta^{e2} & \psi^{e2} \end{bmatrix}^T \\ &= \begin{bmatrix} \mathbf{q}^{cT} & \mathbf{\Phi}^{e1\,T} & \mathbf{\Phi}^{e2\,T} \end{bmatrix}^T \end{aligned} \tag{33}$$

where superscript *CB* stands for the carbody-bogie frames composed body. This set of coordinates is free of constraints. Railway wheelset bodies are connected with revolute joints (bearings) to a pair of axleboxes. With regard to the multibody model, there are two types of wheelset bodies: wheelsets with non-rotating axleboxes and wheelsets with rotating axleboxes, see Fig. 3 on the right. Non-rotating axleboxes are assumed to remain parallel to the WIF, not showing pitch rotation. This is reasonable if the pitch rotation of the axlebox has no interest in the dynamic simulation or little influence in the overall dynamics. This is a valid approximation when primary suspension elements are such that the direction of the forces that they apply point to the wheelset axle.

For other configurations of the primary suspension elements, as shown in Fig. 3 on the right, the accurate calculation of the axlebox pitch rotation is important in the calculation of the suspension forces. In this case the wheelset body includes two additional degrees of freedom associated with the pitch rotations of the two axleboxes. Therefore the wheelset with non-rotating axleboxes has 6 degrees of freedom whereas the wheelset with rotating axleboxes has 8 degrees of freedom. For the wheelset with 6 degrees of freedom, the two axleboxes can be considered as a single body whose position coincides with the position of the WF and its orientation coincides with the WIF. For the wheelset with 8 degrees of freedom the coordinate vector is given by:

$$\begin{aligned} \mathbf{q}^{W} &= \begin{bmatrix} x^w & y^w & z^w & \varphi^w & \theta^w & \psi^w & \theta^{ab1} & \theta^{ab2} \end{bmatrix}^T \\ &= \begin{bmatrix} \mathbf{q}^{wT} & \theta^{ab1} & \theta^{ab2} \end{bmatrix}^T \end{aligned} \tag{34}$$

where superscript *W* stands for the wheelset-axle boxes composed body.

Based on these sets of coordinates, alternative kinematic relations equivalent to Eqs. (10)–(22) can be obtained symbolically. These kinematic relations can be used to obtain the equations of motion of the vehicle from the Newton–Euler equations of the different bodies using an equivalent method to that used in Section 4. For the sake of brevity, the kinematics and dynamics of railroad vehicles that include joint constraints is not reproduced in this article. However, it is important to mention that the use of open-loop coordinates as given in Eqs. (33) and (34) avoids the need of including constraint equations due to kinematic joints.

6. Wheel-rail contact with lookup tables

In the method proposed in this work wheel-rail contact does require the consideration of non-linear constraints. However, these constraints are treated in a very efficient manner using lookup tables. Lookup tables account for the permanent wheel-rail tread contact that is considered as

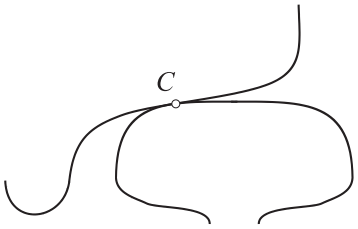

Fig. 4. Arbitrary wheel-rail contact point *C*.

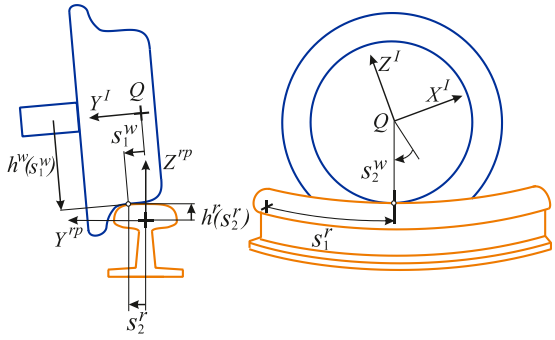

Fig. 5. Wheel/rail surface parameters used for the location of contact points.

perfectly rigid and also for the intermittent wheel-rail flange contact that is considered as an elastic contact, thus allowing interpenetration. This wheel-rail contact method is called *hybrid*.

In the following, the method for treating wheel-rail contact using lookup tables for arbitrary-geometry track including irregularities is explained in detail.

6.1. Contact constraints

The wheel-rail contact shown in Fig. 4 is treated in this work using a set of contact constraints that allow four relative degrees of freedom of the wheelset with respect to the track. A single contact point is assumed for each wheel-rail pair that constrains one degree of freedom of relative motion. The constraint equations at each wheel-rail contact can be written as:

$$\mathbf{C}_j^C\left(\mathbf{q}^w,\mathbf{s}\right)=\begin{bmatrix}\bar{\mathbf{r}}_C^w(\mathbf{q}^w,\mathbf{s}^w)-\bar{\mathbf{r}}_C^r\left(\mathbf{s}^r,s^t\right)\\ \bar{\mathbf{t}}_{1C}^{w\,T}\bar{\mathbf{n}}_C^r\\ \bar{\mathbf{t}}_{2C}^{w\,T}\bar{\mathbf{n}}_C^r\end{bmatrix}=\mathbf{0},\quad j=L,R \tag{35}$$

where L and R stand for left or right wheel-rail contact. The first vector equation (three scalar equations) is called *contact point position constraint* whereas the two last equations represent the *contact point orientation constraints*. These constraint equations are used to impose the non-conformal contact of two bodies with smooth surfaces. Contact point constraints guarantee that there is a point on the wheel, the contact point C on the wheel, that instantaneously occupies the same position in space that other point on the rail, the contact point C on the rail. The contact point orientation constraints guarantee that the tangent plane to the wheel at the contact point is parallel to the tangent plane to the rail at the contact point.

All vectors in Eq. (35) are defined with respect to the TF. The contact point position on the wheel $\bar{\mathbf{r}}_C^w$ and on the rail $\bar{\mathbf{r}}_C^r$ are functions of the surface parameters of the wheel $\mathbf{s}^w=[\ s_1^w\quad s_2^w\ ]^T$ and surface parameters of the rail $\mathbf{s}^r=[\ s_1^r\quad s_2^r\ ]^T$, respectively, as well as on the wheelset position with respect to the TF and on the TF arc-length parameter s^t. Vector $\mathbf{s}=[\ \mathbf{s}^w\quad \mathbf{s}^r\ ]^T$ contains the four surface parameters. The surface parameters are the curvilinear coordinates used to locate an arbitrary point on the surfaces. Their physical meaning is shown in Fig. 5. The position of arbitrary points on the surface of the wheel and the rail with respect to the TF are given by:

$$\begin{aligned}\bar{\mathbf{r}}_C^w&=\bar{\mathbf{r}}^w+\mathbf{A}^{t,wif}\tilde{\mathbf{u}}_C^w\\ \bar{\mathbf{r}}_C^r&=\mathbf{A}^{t\,T}\left(\mathbf{R}_C^r-\mathbf{R}^t\right)\end{aligned} \tag{36}$$

where

$$\begin{aligned}\tilde{\mathbf{u}}_C^w&=\begin{bmatrix}-g\left(s_1^w\right)\sin s_2^w\\ \pm l+s_1^w\\ -g\left(s_1^w\right)\cos s_2^w\end{bmatrix}\\ \mathbf{R}_C^r&=\mathbf{R}^{rp}\left(s_1^r\right)+\mathbf{A}^{rp}\left(s_1^r\right)\begin{bmatrix}0\\ s_2^r\\ f\left(s_2^r\right)\end{bmatrix}\end{aligned} \tag{37}$$

are the position vector of the contact point on the wheel in the WIF and the position of the contact point on the rail in the GF, respectively. In this equation $\mathbf{R}^{rp}$ and $\mathbf{A}^{rp}$ are the global position of the origin and the orientation matrix of a rail profile frame, shown in Fig. 5, which are functions of the arc-length rail parameter s_1^r provided by a track preprocessor, l is the coordinate along the Y^{wif} axis of the center of the wheel and $h^r(s_2^r)$ and $h^w(s_1^w)$ define the rail head and wheel profiles, respectively, as functions of the transverse surface parameters. These functions can be analytically defined or spline functions that extrapolate the coordinates of a set of surface points given in tables. Note that the '±' sign in Eq. (37) for the l distance refers to the right and left wheels respectively.

The 3 vectors that appear in the contact point orientation constraints in Eq. (35) are two tangents to the wheel at the contact point and the normal to the rail at the contact point. They are calculated as follows:

$$\begin{aligned}\bar{\mathbf{t}}_{1C}^w&=\frac{\partial\bar{\mathbf{r}}_C^w}{\partial s_1^w},\quad \bar{\mathbf{t}}_{2C}^w=\frac{\partial\bar{\mathbf{r}}_C^w}{\partial s_2^w}\\ \bar{\mathbf{t}}_{1C}^r&=\frac{\partial\bar{\mathbf{r}}_C^r}{\partial s_1^r},\quad \bar{\mathbf{t}}_{2C}^r=\frac{\partial\bar{\mathbf{r}}_C^r}{\partial s_2^r},\quad \bar{\mathbf{n}}_C^r=\bar{\mathbf{t}}_{1C}^r\times\bar{\mathbf{t}}_{2C}^r\end{aligned} \tag{38}$$

The contact constraints vector $\mathbf{C}_j^C$ given in Eq. (35) includes 5 constraint equations but it also adds 4 new coordinates to the system: the 4 surface parameters associated with the contact point on the wheel ($\mathbf{s}^w$) and on the rail ($\mathbf{s}^r$). Therefore, each wheel-rail contact eliminates (5 – 4 =) 1 degree of freedom of relative motion.

6.2. Wheel-rail contact lookup table

In order to create the wheel-rail contact lookup tables, the contact constraint equations given in Eq. (35) are solved for a set of values of the wheelset coordinates. Every wheelset having one contact point on the left wheel and one contact point on the right wheel is subjected to the 10 contact constraints given by $\mathbf{C}_L^C$ and $\mathbf{C}_R^C$. These constrains are 10 non-linear algebraic equations which are functions of 14 coordinates, the 6 wheelset coordinates given in $\mathbf{q}^w$ plus the 8 surface parameters associated with the two contacts: $\mathbf{s}_L^w$, $\mathbf{s}_L^r$, $\mathbf{s}_R^w$ and $\mathbf{s}_R^r$. However, looking carefully to the contact constraint equations in Eq. (35) one realizes that they do not depend on θ^w since the wheelset contact point local position vector is given in the WIF which does not show pitch rotation. The number of unknowns is thus reduced from 14 to 13.

To create the contact lookup table the contact constraints are solved for the position and orientation of the wheelset with respect to the WTF instead of its position and orientation with respect to the TF. This is, using $\mathbf{q}^{wif}$ (defined in Eq. (7)) instead of $\mathbf{q}^w$. It is easy to understand that the wheel-rail contact can only be tabulated with respect to a frame that closely follows its motion, like the WTF. However, the wheelset can be at any distance and show any orientation with respect to the TF. Because $\mathbf{q}^{wif}$ contains 5 coordinates instead of 6 ($x^{wif}=0$) the number of unknowns is thus reduced from 13 to 12.

To form the lookup table numerical values are given to the coordinates y^{wif} and ψ^{wif}, and the 10 non-linear algebraic equations $\mathbf{C}_L^C$ and $\mathbf{C}_R^C$ are solved to provide 10 unknowns: the remaining wheelset coordinates z^{wif} and φ^{wif}, and the 8 surface parameters $\mathbf{s}_L^w$, $\mathbf{s}_L^r$, $\mathbf{s}_R^w$ and $\mathbf{s}_R^r$. Therefore, the lookup table has two entries (y^{wif} and ψ^{wif}) and it provides, among

other data, the vertical wheelset displacement and roll angle, as follows:

$$\begin{aligned} z^{wif} &= f\left(y^{wif}, \psi^{wif}\right) \\ \varphi^{wif} &= g\left(y^{wif}, \psi^{wif}\right) \end{aligned} \tag{39}$$

If the wheelset yaw angle is small, as it usually occurs in railroad dynamics, the dependency of the vertical displacement and the roll angle on it is insignificant. Thus, for simplicity, one can assume that there is no such dependency, as follows:

$$\begin{aligned} z^{wif} &\approx f\left(y^{wif}, 0\right) = f\left(y^{wif}\right) \\ \varphi^{wif} &\approx g\left(y^{wif}, 0\right) = g\left(y^{wif}\right) \end{aligned} \tag{40}$$

The number of entries of the look-up table is thus reduced from 2 to 1. Due to the contact constraints, the position of the origin and orientation of the WIF with respect to the WTF, given at Eq. (8) become:

$$\widehat{\mathbf{b}}^{w} = \begin{bmatrix} 0 \\ y^{wif} \\ f(y^{wif}) \end{bmatrix}, \mathbf{A}^{wtf,wif} = \begin{bmatrix} 1 & -\psi^{wif} & \theta^{wif} \\ \psi^{wif} & 1 & -g(y^{wif}) \\ -\theta^{wif} & g(y^{wif}) & 1 \end{bmatrix} \tag{41}$$

The two independent wheelset constraint equations due to wheel-rail contact can be extracted from the expressions of the 'z' component of vector $\bar{\mathbf{r}}^{w}$ and term (3,2) (third row, second column) of the transformation matrix $\mathbf{A}^{t,wif}$ given in Eq. (9), as follows:

$$\begin{aligned} & z^{w} - \left(z^{wif} + \mathbf{A}_{r3}^{t,wtf} \begin{bmatrix} 0 \\ y^{wif} \\ f(y^{wif}) \end{bmatrix} \right) = 0 \\ & \mathbf{A}_{c3}^{t,wtf\,T} \mathbf{A}_{c2}^{t,wif}(\mathbf{q}^{w}) - g(y^{wif}) = 0 \end{aligned} \tag{42}$$

where $\mathbf{A}_{r3}^{t,wtf}$ and $\mathbf{A}_{c3}^{t,wtf}$ are the third row and third column of $\mathbf{A}^{t,wtf}$, respectively, and $\mathbf{A}_{c2}^{t,wif}$ is the second column of $\mathbf{A}^{t,wif}$. Eq. (42) contains the two general non-linear constraint equations of the wheelset due to wheel-rail contact implemented with lookup tables ($f(y^{wif})$, $g(y^{wif})$) in a general-geometry track. They can be written in the compact form as:

$$\mathbf{C}^{wr}\left(\mathbf{q}^{w}\right) = \mathbf{0} \tag{43}$$

where superscript *wr* refers to wheel-rail constraints. Eq. (42) represents the general wheelset-track contact constraints in the case of a single contact point on each wheel. In the particular case of a tangent track ($\mathbf{A}^{t,wtf} = \mathbf{I}$) without vertical slope ($z^{wif} = 0$, $y^{wif} = y^{w}$) Eq. (42) reduces to:

$$\begin{aligned} & z^{w} - f(y^{w}) = 0 \\ & \sin\varphi^{w} - g(y^{w}) = 0 \end{aligned} \tag{44}$$

This form is clearly consistent with Eq. (40) under the small-angles assumption.

6.3. Derivatives of the contact constraints with lookup tables

Constraint equations in multibody dynamics have to be treated at position level, as given in Eq. (42), but also at velocity level and acceleration level. In the case of holonomic and scleronomic constraints the velocity and acceleration level equations yield:

$$\begin{aligned} & \mathbf{C}_{\mathbf{q}w}^{wr} \dot{\mathbf{q}}^{w} = \mathbf{0} \\ & \mathbf{C}_{\mathbf{q}w}^{wr} \ddot{\mathbf{q}}^{w} + \dot{\mathbf{C}}_{\mathbf{q}w}^{wr} \dot{\mathbf{q}}^{w} = \mathbf{0} \end{aligned} \tag{45}$$

where

$$\begin{aligned} \mathbf{C}_{\mathbf{q}w}^{wr} &= \frac{\partial \mathbf{C}^{wr}}{\partial \mathbf{q}^{w\,T}}, \\ \dot{\mathbf{C}}_{\mathbf{q}w}^{wr} &= \frac{d\mathbf{C}_{\mathbf{q}}^{wr}}{dt} = \frac{\partial\left(\mathbf{C}_{\mathbf{q}}^{wr}\dot{\mathbf{q}}^{w}\right)}{\partial \mathbf{q}^{w\,T}} \end{aligned} \tag{46}$$

The 2 matrices that appear in this equation have to be evaluated with the help of the contact lookup tables too. The symbolic computation of these matrices requires the computation of the partial derivatives s^{wtf} and y^{wif} with respect to $\mathbf{q}^{w}$ and in practice this is a very complicated task. In this work, the dependency of s^{wtf} with $\mathbf{q}^{w}$ is neglected. This is equivalent to assume that during the vehicle motion the WTF is at a constant distance to the TF along the track regardless of the coordinates $\mathbf{q}^{w}$. This is not exact (that is why Eq. (6) should be solved each time step) but reasonable for the calculation of the Jacobian matrix of the constraints. With regard to the lateral displacement y^{wif} the following partial derivative is obtained from Eq. (9):

$$\frac{\partial y^{wif}}{\partial \mathbf{q}^{w\,T}} = \begin{bmatrix} \mathbf{A}_{c2}^{t,wtf\,T} & 0 & 0 & 0 \end{bmatrix} \tag{47}$$

Calling C_1^{wr} and C_2^{wr} to the two general constraint equations in Eq. (42), the rows of the contact constraint Jacobian matrix $\mathbf{C}_{\mathbf{q}w}^{wr}$ become:

$$\begin{aligned} \frac{\partial C_1^{wr}}{\partial \mathbf{q}^{w\,T}} &= \begin{bmatrix} 0 & 0 & 1 & 0 & 0 & 0 \end{bmatrix} - \mathbf{A}_{r3}^{t,wtf} \begin{bmatrix} 0 \\ 1 \\ f'(y^{wif}) \end{bmatrix} \frac{\partial y^{wif}}{\partial \mathbf{q}^{w\,T}} \\ \frac{\partial C_2^{wr}}{\partial \mathbf{q}^{w\,T}} &= \mathbf{A}_{c3}^{t,wtf\,T} \frac{\partial \mathbf{A}_{c2}^{t,wif}}{\partial \mathbf{q}^{w\,T}} - g'(y^{wif}) \frac{\partial y^{wif}}{\partial \mathbf{q}^{w\,T}} \end{aligned} \tag{48}$$

where f' and g' are the derivatives of the lookup table functions with respect to the input parameter y^{wif} and the Jacobian matrix $\frac{\partial \mathbf{A}_{c2}^{t,wif}}{\partial \mathbf{q}^{w\,T}}$ is given by:

$$\frac{\partial \mathbf{A}_{c2}^{t,wif}}{\partial \mathbf{q}^{w\,T}} = \begin{bmatrix} 0 & 0 & 0 & \sin\psi^{w}\sin\varphi^{w} & 0 & -\cos\psi^{w}\cos\varphi^{w} \\ 0 & 0 & 0 & -\cos\psi^{w}\sin\varphi^{w} & 0 & -\sin\psi^{w}\cos\varphi^{w} \\ 0 & 0 & 0 & \cos\varphi^{w} & 0 & 0 \end{bmatrix} \tag{49}$$

The time derivative of the two terms in Eq. (48) provides the rows of the matrix $\dot{\mathbf{C}}_{\mathbf{q}w}^{wr}$, as follows:

$$\begin{aligned} \frac{d}{dt}\left(\frac{\partial C_1^{wr}}{\partial \mathbf{q}^{w\,T}}\right) &= -\dot{\mathbf{A}}_{r3}^{t,wtf} \begin{bmatrix} 0 \\ 1 \\ f'(y^{wif}) \end{bmatrix} \frac{\partial y^{wif}}{\partial \mathbf{q}^{w\,T}} \\ & -\mathbf{A}_{r3}^{t,wtf} \left(\begin{bmatrix} 0 \\ 0 \\ f''(y^{wif}) \end{bmatrix} \frac{\partial y^{wif}}{\partial \mathbf{q}^{w\,T}} \dot{\mathbf{q}}^{w} \frac{\partial y^{wif}}{\partial \mathbf{q}^{w\,T}} + \begin{bmatrix} 0 \\ 1 \\ f'(y^{wif}) \end{bmatrix} \frac{d}{dt}\left(\frac{\partial y^{wif}}{\partial \mathbf{q}^{w\,T}}\right) \right) \\ \frac{d}{dt}\left(\frac{\partial C_2^{wr}}{\partial \mathbf{q}^{w\,T}}\right) &= \dot{\mathbf{A}}_{c3}^{t,wtf\,T} \frac{\partial \mathbf{A}_{c2}^{t,wif}}{\partial \mathbf{q}^{w\,T}} + \mathbf{A}_{c3}^{t,wtf\,T} \frac{d}{dt}\left(\frac{\partial \mathbf{A}_{c2}^{t,wif}}{\partial \mathbf{q}^{w\,T}}\right) \\ & -g''(y^{wif}) \frac{\partial y^{wif}}{\partial \mathbf{q}^{w\,T}} \dot{\mathbf{q}}^{w} \frac{\partial y^{wif}}{\partial \mathbf{q}^{w\,T}} - g'(y^{wif}) \frac{d}{dt}\left(\frac{\partial y^{wif}}{\partial \mathbf{q}^{w\,T}}\right) \end{aligned} \tag{50}$$

where f'' and g'' are the second derivatives of the lookup table functions with respect to the input parameter y^{wif}.

In the particular case of a tangent track ($\mathbf{A}^{t,wtf} = \mathbf{I}$) without vertical slope ($z^{wif} = 0$, $y^{wif} = y^{w}$) matrices $\mathbf{C}_{\mathbf{q}w}^{wr}$ and $\dot{\mathbf{C}}_{\mathbf{q}w}^{wr}$ reduces to:

$$\begin{aligned} \mathbf{C}_{\mathbf{q}w}^{wr} &= \begin{bmatrix} 0 & -f' & 1 & 0 & 0 & 0 \\ 0 & -g' & 0 & \cos\varphi^{w} & 0 & 0 \end{bmatrix} \\ \dot{\mathbf{C}}_{\mathbf{q}w}^{wr} &= \begin{bmatrix} 0 & -f''\,\dot{y}^{w} & 0 & 0 & 0 & 0 \\ 0 & -g''\,\dot{y}^{w} & 0 & -\sin\varphi^{w}\dot{\varphi}^{w} & 0 & 0 \end{bmatrix} \end{aligned} \tag{51}$$

6.4. Calculation of generalized normal contact forces with lookup tables

Since the wheel-rail contact is accounted for in this formulation using a constraint approach, the generalized wheel-rail normal contact forces appear in the equations of motion as reaction forces associated with these constraints, as follows:

$$\mathbf{Q}_{con}^{n} = -\mathbf{C}_{\mathbf{q}}^{wr\,T} \boldsymbol{\lambda}^{wr} \tag{52}$$

where the global Jacobian matrix $\mathbf{C}_{\mathbf{q}}^{wr}$ is obtained by assembling the Jacobian matrices $\mathbf{C}_{\mathbf{q}w1}^{wr}$, $\mathbf{C}_{\mathbf{q}w2}^{wr}$, ...$\mathbf{C}_{\mathbf{q}wp}^{wr}$ associated with all wheelsets in the vehicle, where p is the total number of wheelsets in the vehicle. Vector $\boldsymbol{\lambda}^{wr}$ in Eq. (52) is the vector of Lagrange multipliers associated with the contact constraints. This expression of the generalized normal contact forces is now inserted into the equations of motion of the vehicle given in Eq. (31). Augmenting the resulting equations with the constraint equations yield:

$$\begin{aligned} & \mathbf{M}\ddot{\mathbf{q}} + \mathbf{C}_{\mathbf{q}}^{wr\,T} \boldsymbol{\lambda}^{wr} = \mathbf{Q} + \mathbf{Q}_{v} + \mathbf{Q}_{TFin} + \mathbf{Q}_{susp} \\ & \mathbf{C}^{wr}(\mathbf{q}) = \mathbf{0} \end{aligned} \tag{53}$$

where $\mathbf{C}^{wr}$ in this equation is not the set of 2 constraint equations given in Eqs. (42) and (43) but the assembly of $2p$ contact constraint equations

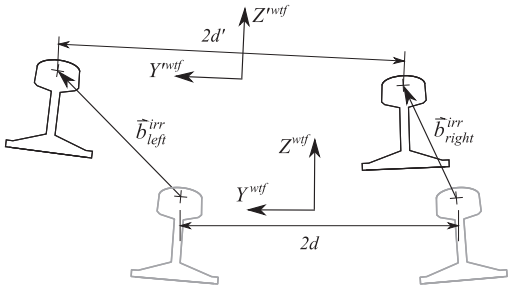

Fig. 6. Definition of track irregularities. The ideal position of the left and right rail cross sections can be observed in grey while the actual positions are shown in black. The lateral and vertical components of the cross-sections displacements represent a measure of the track irregularities.

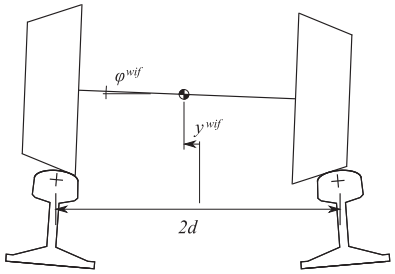

Fig. 7. Wheelset coordinates associated with lateral dynamics with respect to the WIF: lateral displacement y^{wif} and roll angle φ^{wif}.

associated with each wheelset and treated with lookup tables. The equations of motion have become a system of *differential-algebraic equations* (DAE).

6.5. Use of lookup tables with track irregularities

Simulation of track irregular geometry is essential in railroad dynamics since this is the main source of vehicle vibrations [18]. Fig. 6 shows a track section. The ideal positions of the rails cross-sections are represented in grey while their actual positions are shown in black. The components of the displacement vectors $\vec{b}^{irr}_{left}$ and $\vec{b}^{irr}_{right}$ in the WTF can be used to compute the four track irregularities associated with the rail heads centerlines, as follows:

- Alignment: $al(s) = \dfrac{\left[\bar{\mathbf{b}}^{irr}_{left}\right]_y + \left[\bar{\mathbf{b}}^{irr}_{right}\right]_y}{2}$
- Vertical profile: $vp(s) = \dfrac{\left[\bar{\mathbf{b}}^{irr}_{left}\right]_z + \left[\bar{\mathbf{b}}^{irr}_{right}\right]_z}{2}$
- Gauge variation: $gv(s) = \left[\bar{\mathbf{b}}^{irr}_{left}\right]_y - \left[\bar{\mathbf{b}}^{irr}_{right}\right]_y$
- Cross level: $cl(s) = \left[\bar{\mathbf{b}}^{irr}_{left}\right]_z - \left[\bar{\mathbf{b}}^{irr}_{right}\right]_z$

where the components of these vectors are given in an ideal-geometry TF.

In order to deal with track irregularities, the number of entries in the lookup table has to be increased from one to two. Out of the four track irregularities it is clear that the only one that has an influence in the wheel-rail contact is the gauge variation gv. Therefore, gv is used as a new entry in the lookup table. To create the lookup table, the wheel-rail contact constraints have to be solved as a function of the lateral displacement of the wheelset for a set of admissible values of the gauge variation gv. In this case the lookup table contains pre-computed values of the following functions:

$$\begin{aligned} z^{wif} &= f\left(y^{wif}, gv\right) \\ \varphi^{wif} &= g\left(y^{wif}, gv\right) \end{aligned} \tag{54}$$

There are two possible ways to simulate the motion of a wheelset on an irregular track. They depend on whether the track preprocessor that provides the absolute position and orientation of the TF (or WTF) as a function of the arc-length s^t (or s^{wtf}) returns the values of the ideal-geometry frame ($[X^{wtf}, Y^{wtf}, Z^{wtf}]$ or the irregular geometry frame ($[X'^{wtf}, Y'^{wtf}, Z'^{wtf}]$ (see Fig. 6). In the latter case the lookup table just requires as an input the value of gv. In the former case the solution is simple too but more elaborate. The position and orientation of the WIF with respect to the ideal or irregular WTF's (see Fig. 7) are related by:

$$\begin{aligned} y^{wif} &= y'^{wif} + al\left(s^{wtf}\right) \\ z^{wif} &= z'^{wif} + vp\left(s^{wtf}\right) \\ \varphi^{wif} &= \varphi'^{wif} + \frac{cl\left(s^{wtf}\right)}{2d} \end{aligned} \tag{55}$$

If the rail preprocessor provides the position and orientation of an ideal-geometry WTF, the lookup table must be interpreted as:

$$\begin{aligned} z'^{wif} &= f(y'^{wif}, gv) \\ \varphi'^{wif} &= g(y'^{wif}, gv) \end{aligned} \tag{56}$$

and the inputs and outputs of the table has to be calculated according to Eq. (55).

6.6. Flange contact with lookup tables

In the method developed in this work the wheel-flange contact with the rail is considered using an elastic method. In this method the wheel surface penetrates during the simulation in the rail head surface and the contact force is calculated as a function of the measured penetration and velocity of penetration using a Hunt-Crossley [19] continuous normal contact force model. When creating the lookup table, the lateral displacement of the wheel with respect to the rail y^{wif} is varied in a range such that in the limits there is a maximum admissible flange-rail penetration in the left and right wheel-rail contacts. Since the lookup tables are created for different values of the track gauge variation gv, the end values of y^{wif} used to create the lookup tables change accordingly. This is clear because the wheel-track clearance or maximum lateral excursion of the wheelset increases as the gauge increases.

Fig. 8 shows the initial wheel-rail position during the calculation of a lookup table in a track with $d = 0.75$ m and $gv = 3$ mm. Tread and flange are considered as two different surfaces and represented with green and black lines, respectively. As it can be observed there is penetration (maximum admissible) in right wheel while the clearance is large in the left wheel flange-rail contact. From this starting point the wheelset is laterally moved to the left until reaching the same penetration in the left wheel flange-rail contact. The fact that left and right rails are switched in the plot is not an error but a consequence of using a y track axis that points toward the left while plotting software naturally plots abscissa pointing toward the right.

During the generation of the lookup tables, whenever the lateral position of the wheel is such that flange contact occurs, the position of the points of maximum indentation on the wheel flange and the rail head is obtained. This calculation is done solving a set of 4 nonlinear constraint equations [6] that provide the four surface parameters of the points on the wheel and rail that show maximum penetration: $\mathbf{s}^w_F, \mathbf{s}^r_F$, as follows:

$$\begin{aligned} \bar{\mathbf{t}}^{w\,T}_{1C}\left(\bar{\mathbf{r}}^w_C - \bar{\mathbf{r}}^r_C\right) &= 0 \\ \bar{\mathbf{t}}^{w\,T}_{2C}\left(\bar{\mathbf{r}}^w_C - \bar{\mathbf{r}}^r_C\right) &= 0 \\ \bar{\mathbf{t}}^{w\,T}_{1C}\bar{\mathbf{n}}^r_C &= 0 \\ \bar{\mathbf{t}}^{w\,T}_{2C}\bar{\mathbf{n}}^r_C &= 0 \end{aligned} \tag{57}$$

Flange penetration δ is calculated as the distance between these two points. The points of maximum penetration are considered as the contact points on the wheel flange and rail head during the simulations.

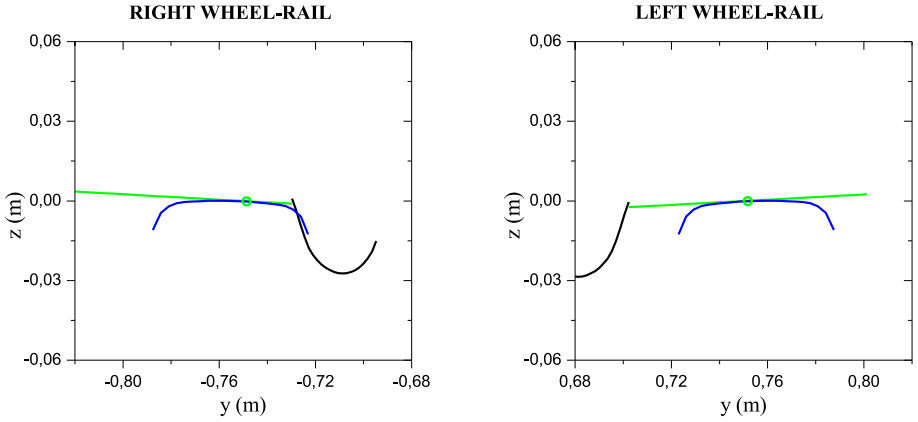

Fig. 8. An arbitrary position of wheel and rail profiles in the generation of contact lookup tables. Blue line: railhead profile. Green line: wheel tread. Black line: wheel flange. The lookup table includes geometric quantities associated with the wheel-rail in contact in a set of relative positions as the one shown in the figure. (For interpretation of the references to color in this figure legend, the reader is referred to the web version of this article.)

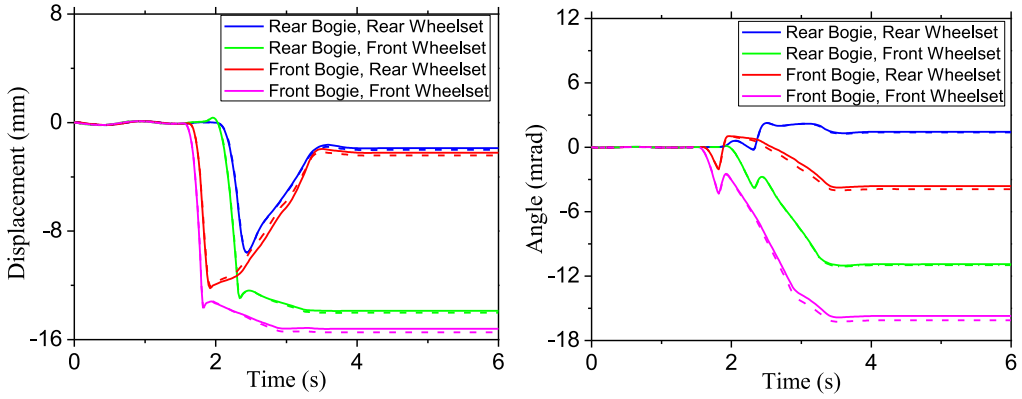

Fig. 9. Simulated wheelset kinematics during small-radius curve negotiation. Solid lines: solution with lookup tables. Dashed lines: solution with contact constraints. Left: wheelsets lateral displacement. Right: wheelsets yaw angle. Wheelsets start the simulation in a tangent track. The transition from tangent to curved track and their final equilibrium positions at the curve are shown.

6.7. Inputs to create the lookup tables

The creation of the lookup table requires the following inputs:

1. Rail profile geometry: function $f(s_2^r)$ defined in Eq. (37) and shown in Fig. 5. Functions are naturally symmetric with respect to the Z^{rp} axis and the same for the left and right rails. These functions can be analytically-defined or the results of the spline-interpolation of a set of points given in tables.
2. Wheel profiles geometry: function $g(s_1^w)$ defined in Eq. (37) and shown in Fig. 5. Functions for the left and right wheels are naturally mirror-symmetric with respect to each other. These functions can be analytically-defined or the results of the spline-interpolation of a set of points given in tables.
3. Track geometric constants: nominal half-gauge d, and cant angle of the rails β.
4. Wheelset geometric constants: half-width of the wheelset l defined in Eq. (37).
5. Track irregularity constants: maximum and minimum values of track gauge variation: gv_{max}, gv_{min}.

6.8. Geometric values included in the lookup tables

A number of n_{gv} lookup tables are computed for a set of discrete values of the gauge variation gv in the range $[-gv_{min}\ gv_{max}]$. For each gauge value the contact constraints are solved for a set of n_y values of the lateral displacement of the wheelset y^{wif} in the range $[-y_{max}]$, where the maximum lateral displacement y_{max} depends on the value gauge variation gv. As explained in Section 6.6, y_{max} is such that it produces a maximum admissible value of flange penetration. In order to calculate the value of y_{max} as a function of gv the left and right rail contact constraints are augmented with a new set of left-flange contact constraints to find the exact lateral displacement to achieve zero penetration in the flange. This problem is solved for each value of gv. Once this problem is solved y_{max} is obtained as this zero-flange penetration displacement plus the maximum admissible penetration.

In total, contact constraint equations are solved $n_{gv} \times n_y$ times to create the lookup tables. Each solution of the contact constraints is done for a particular value of y^{wif} and gv. The following data is stored:

1. Track coordinates: $f = z^{wif}$ and $g = \varphi^{wif}$ (2 scalar values)
2. First space-derivative of track coordinates: $f' = \frac{dz^{wif}}{dy^{wif}}$ and $g' = \frac{d\varphi^{wif}}{dy^{wif}}$. (2 scalar values)
3. Second space-derivative of track coordinates: $f'' = \frac{d^2z^{wif}}{d(y^{wif})^2}$ and $g'' = \frac{d^2\varphi^{wif}}{d(y^{wif})^2}$. (2 scalar values)
4. Contact parameters for left tread contact point $\mathbf{s}_L^w$, $\mathbf{s}_L^r$, right tread contact points, $\mathbf{s}_R^w, \mathbf{s}_R^r$ and points of maximum penetration in flange contact (left or right, whichever shows penetration, if any) $\mathbf{s}_F^w, \mathbf{s}_F^r$. (12 scalar values)
5. Local position vector of contact points in WIF: $\breve{\mathbf{u}}_L^w$, $\breve{\mathbf{u}}_R^w$, $\breve{\mathbf{u}}_F^w$. (9 scalar values)
6. Tangent vectors at contact points in WIF: $\breve{\mathbf{t}}_{1L}^w$, $\breve{\mathbf{t}}_{2L}^w$, $\breve{\mathbf{t}}_{1R}^w$, $\breve{\mathbf{t}}_{2R}^w$, $\breve{\mathbf{t}}_{1F}^w$, $\breve{\mathbf{t}}_{2F}^w$. (18 scalar values)

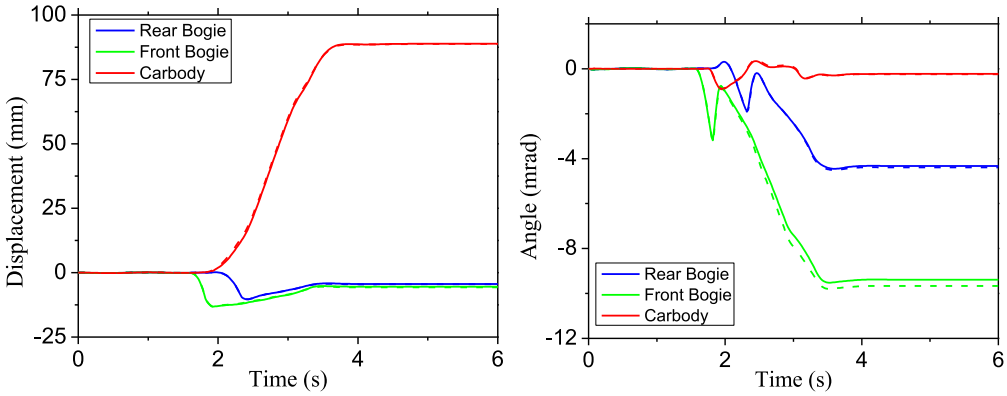

Fig. 10. Simulated carbody and bogie frames kinematics during small-radius curve negotiation. Solid lines: solution with lookup tables. Dashed lines: solution with contact constraints. Left: bogies and carbody lateral displacement. Right: bogies and carbody yaw angle. The transition from tangent to curved track to curve and the final equilibrium positions of bogies and carbody vehicles are shown.

7. Longitudinal and transverse curvatures of the surfaces at contact points: κ^w_{1L}, κ^w_{2L}, κ^w_{1R}, κ^w_{2R}, κ^w_{1F}, κ^w_{2F}. (6 scalar values)
8. Flange penetration δ if any. (1 scalar value)

A total of 52 scalar values have to be stored for each solution of the contact constraints. These values are needed for:

- Calculate the Jacobian of the contact constraints (Eq. (48)) and its time derivative (Eq. (50).)
- Calculate the creepages (non-dimensional velocities) at contact points needed for the calculation of the tangential creep forces.
- Calculate the creepage coefficients needed for the calculation of the tangential creep forces.
- Calculate normal and tangential velocity of flange contact point needed for the calculation of flange normal and tangential contact forces.

7. Simulation results and discussion: efficiency and accuracy of contact lookup tables

The goal of this section is two-fold:

1 To show that the general formulation presented for the simulation of railway vehicles works, and
2 To measure the loss in accuracy and gain in computational efficiency due to the use of contact lookup tables.

The loss of accuracy due to the use of contact lookup tables is due to two main reasons:

1 Because of the errors introduced in the geometry due to numerical interpolation, and
2 Because the influence of the wheelset-track relative yaw (angle of attack) in the contact geometry is neglected.

It is well known that the effect of the wheelset-track relative yaw can be important in case of small-radius curves. Motion along a small-radius curve is particularly important to simulate accurately because it is a clear case of possible derailment due to wheel climbing. This is the reason why in the simulations presented in this section the negotiation of a small-radius curve of a railway vehicle at a relatively large velocity has been selected. Results compare the vehicle motion simulated with lookup tables with the motion simulated with online solution of constraint equations for the tread and elastic contact for the flanges.

In the numerical results the model of the vehicle ML95 (Lisbon subway company) that are used in [20] is simulated. Inertia, geometry and stiffness and damping parameters can be found in that reference. This vehicle has the common configuration of one carbody connected by secondary suspensions to two bogies each of which includes a bogie frame connected by a primary suspension with two rigid-axle wheelsets. Wheel-rail profiles geometry is also taken from [20]. The track geometry includes a tangent segment of 60 m, followed by a transition segment of 40 m, followed by a curved track with $R = 165$ m and no superelevation. The forward velocity of the vehicle is assumed constant $V = 30$ m/s. In order to simulate a steady curve negotiation of the vehicle the track is assumed free of irregularities.

Fig. 9 shows the lateral displacement and yaw angles of the vehicle wheelsets. Fig. 10 shows the results for the bogie frames and carbody. One can clearly observe the effect of the entrance in the curve and the achievement of the steady curving. Solid lines correspond to the solution with lookup tables (LU) while dashed lines correspond to the solution with contact constraints (CC). These results are quantified in Table 1 for the steady curving. Note that in this table, superscript *bif* refers to "body intermediate frame", which is similar to wheelset intermediate frame but more general, since not all bodies are wheelsets. One can conclude that both methods produce similar results, being the maximum relative error 9.1% and the average relative error 3.7%.

The computational efficiency of the use of lookup tables is now evaluated. The simulation has been performed using an in-house computer code developed in Matlab R2016a with a computer with processor Inter Xeon CPU E5520 @ 2.27 GHz. The code is not optimized for computational efficiency so *Mex functions* written in C or Fortran are not used. Matlab integrators with default parameters are used for numerical integration. An exception is *ode4* which is an explicit fourth order Runge–Kutta integrator that was originally developed by Matlab but it is no longer distributed. However, this function is easily downloaded from Matlab web. Integration times are given in Table 2.

All integrators use automatically adjusted variable time step with the exception of *ode4* that uses constant time step. In this case the time step was fixed to 1 ms. The use of *ode4* is then convenient for objectivity in the calculation of the relative computational efficiency. Integrator *ode15s* that is specific for stiff problems fails to converge at the instant of entrance to the curve when using contact constraints. This fact is attributed to the difficulty to deal with the wheel flange contact that first occurs at that instant. It can be observed that the use of lookup tables avoids the necessity of solving the nonlinear contact constraints (constraint approach for the tread and elastic one for the flange) during the dynamic simulation of railway vehicles and results in simulations which are six times faster that simulations based on the online solution of contact constraints. Getting with this non-optimized Matlab code a ratio of (49/6 =) 8.2 s of integration per real-time second it is not risky to conclude that the proposed method could simulate the motion of this vehicle in real time if implemented in C or Fortran and/or little computational optimization.

Table 1
Vehicle coordinates during steady curving.

	Rear wh., rear bogie	Front wh. rear bogie	Rear wh., front bogie	Front wh., front bogie	Rear bogie	Front bogie	Carbody
y^{bif}, LU (mm)	−1.89	−13.87	−2.22	−15.20	−4.39	−5.47	88.84
y^{bif}, CC (mm)	−2.01	−14.01	−2.42	−15.46	−4.52	−5.71	88.76
Error	6.62%	1.02%	9.10%	1.67%	3.06%	4.26%	0.09%
ψ^{bif}, LU (mrad)	1.44	−10.89	−3.61	−15.71	−4.32	−9.38	−0.23
ψ^{bif}, CC (mrad)	1.38	−10.98	−3.89	−16.12	−4.39	−9.67	−0.24
Error	4.22%	0.84%	7.81%	2.62%	1.46%	3.04%	6.53%

Table 2
Integration times.

Integrator/Contact model	Lookup Tables	Contact constraints	Time CC/Time LU
ode45	327 s	1992 s	6.1
ode113	230 s	1334 s	5.8
ode4	898 s	6132 s	6.8
ode15s	49 s	–	–

8. Conclusion

This paper starts with a discussion of the benefits and drawbacks of the use of absolute coordinates referred to a global frame or relative coordinates referred to a non-inertial track frame in multibody railway simulations. This work supports the use of relative coordinates and adopts a solution that requires a unique track frame to describe the motion of the whole vehicle. Up to five different types of frame are needed to analyze the motion of the vehicle bodies.

Kinematic analysis with relative coordinates is more involved than kinematic analysis with global coordinates. This paper presents a systematic procedure for the symbolic calculation of the bodies' velocities and accelerations as a function of the generalized coordinates and their time derivatives. The resulting expressions are based on the use of the Jacobian of the position and orientation of the bodies with respect to the generalized coordinates and velocities. These Jacobian matrices are also used in the calculation of the equations of motion of the vehicle out of the Newton–Euler equations of motion of the vehicle bodies. The paper applies this procedure to vehicle models that exclude kinematic joints between the vehicle bodies. In case kinematic joints do exist an alternative kinematic analysis is proposed that models the vehicle as a set of open-chain multibody system with relative coordinates.

Contact lookup tables can be created using different assumptions related to the wheel-rail contact. The contact lookup tables used in this work assume constraint contact in the wheel tread and elastic contact in the wheel flange. The influence of the yaw angle in the wheel-rail contact geometry is neglected. Lookup tables are developed such that they can be used for the simulation of wheelsets running on irregular tracks. Finally a lookup table with just two entries, the lateral displacement and the track gauge variation, is developed to provide all the required information to simulate the wheel rail tread and flange contacts in a track with arbitrary geometry.

Numerical simulations compare the use of the contact lookup tables with the direct solution of the wheel-rail contact constraints. To this end, the scenario in which a complete vehicle negotiates a small-radius curve with a high forward velocity has been selected. In this scenario the influence of the wheel yaw angle on the contact conditions can be particularly important on the curving performance of the vehicle. Simulations show that the use of contact lookup tables provide relatively accurate results in this extreme situation. Results show that, measured by CPU-times, the computational efficiency when using contact lookup tables is six times better than the computational efficiency of the direct use of contact constraints.

Acknowledgment

This research was supported by the Spanish Ministry of Economy, Industry and Competitiveness (MINECO) under the project TRA2017-86355-C2-1-R. This support is gratefully acknowledged.

References

[1] Escalona JL, Park T-W, Zaazaa KE. Railroad vehicle dynamics—A roadmap to high speed trains. J Comput Nonlinear Dyn 2012;7(4).
[2] Cuadrado J, Dopico D, Naya MA, González M. Penalty, semi-recursive and hybrid methods for MBS real-time dynamics in the context of structural integrators. Multibody Syst Dyn 2004;12(2):117–32.
[3] Shabana AA, Zaazaa KE, Sugiyama H. Railroad vehicle dynamics: a computational approach. CRC Press; 2007.
[4] Shabana AA, Tobaa M, Sugiyama H, Zaazaa KE. On the computer formulations of the wheel/rail contact problem. Nonlinear Dyn 2005;40(2):169–93.
[5] Shabana AA, Sany JR. An augmented formulation for mechanical systems with non–generalized coordinates: application to rigid body contact problems. Nonlinear Dyn 2001;24(2):183–204.
[6] Shabana AA, Zaazaa KE, Escalona JL, Sany JR. Development of elastic force model for wheel/rail contact problems. J Sound Vib 2004;269(1):295–325.
[7] Malvezzi M, Meli E, Falomi S, Rindi A. Determination of wheel–rail contact points with semianalytic methods. Multibody Syst Dyn 2008;20(4):327–58.
[8] Auciello J, Meli E, Falomi S, Malvezzi M. Dynamic simulation of railway vehicles: wheel/rail contact analysis. Veh Syst Dyn 2009;47(7):867–99.
[9] Sugiyama H, Araki K, Suda Y. On-line and off-line wheel/rail contact algorithm in the analysis of multibody railroad vehicle systems. J Mech Sci Technol 2009;23(4):991–6.
[10] Recuero AM, Aceituno JF, Escalona JL, Shabana AA. A nonlinear approach for modeling rail flexibility using the absolute nodal coordinate formulation. Nonlinear Dyn 2016;83(1-2):463–81.
[11] Schupp G, Weidemann C, Mauer L. Modelling the contact between wheel and rail within multibody system simulation. Veh Syst Dyn 2004;41(5):349–64.
[12] Rulka W. SIMPACK—A computer program for simulation of large-motion multibody systems. In: Multibody systems handbook. Heidelberg: Springer; 1990. p. 265–84.
[13] Meli E, Malvezzi M, Papini S, Pugi L, Rinchi M, Rindi A. A railway vehicle multibody model for real-time applications. Veh Syst Dyn 2008;46(12):1083–105.
[14] Santamaría J, Vadillo EG, Gómez J. A comprehensive method for the elastic calculation of the two-point wheel–rail contact. Veh Syst Dyn 2006;44(sup1):240–50.
[15] Popp K, Schiehlen W. Ground vehicle dynamics. Springer Science & Business Media; 2010.
[16] Escalona JL, Chamorro R, Recuero AM. Description of methods for the eigenvalue analysis of railroad vehicles including track flexibility. J Comput Nonlinear Dyn 2012;7(4).
[17] Shabana AA. Computational dynamics. John Wiley & Sons; 2009.
[18] Garg V. Dynamics of railway vehicle systems. Elsevier; 2012.
[19] Hunt KH, Crossley FRE. Coefficient of restitution interpreted as damping in vibro-impact. ASME J. Appl Mech 1975:440–5.
[20] Pombo J, Ambrosio J. Dynamic analysis of a railway vehicle in real operation conditions using a new wheel-rail contact detection model. Int J Veh Syst Model Testing 2005;1(1-3):79–105.